Modeling and Analysis of a Wide-Speed-Range Induction Motor Drive Based on Electronic Pole Changing

Mohamed Osama, *Member, IEEE,* and Thomas A. Lipo, *Fellow, IEEE*

***Abstract*— It has been previously demonstrated that an induction machine drive with contactorless pole changing can be achieved by reversing current directions of certain stator coil groups. This paper compares the power and torque capability of this drive with conventional four-pole and two-pole induction machine drives. Based on the technique of vector space decomposition, the machine coupled-circuit model is transformed to a reference frame model. As a result of this transformation, the coupled coil group variables can be replaced by equivalent decoupled four-pole and two-pole $dq0$ variables. This reference frame model facilitates the analysis and control of the machine drive, especially during transients, such as the pole-changing transition.**

***Index Terms*—Electronic pole changing, reference frame model, induction motor.**

I. INTRODUCTION

SEVERAL applications, such as electric vehicles and spindle drives, require a drive capable of both high torque at low speeds and a wide constant-horsepower speed range (4 or 5 to 1). Previous approaches to meet these requirements either needed winding connection switching devices, oversizing of the machine and/or inverter, or modifying the machine magnetic structure design. Switching devices, which can be either a magnetic contactor or solid-state switches, degrade the drive dynamic performance and present an additional cost. Space constraints in certain drives make oversizing the machine nonfeasible, while oversizing the inverter is uneconomical. Modifying the machine magnetic structure to decrease the leakage inductance and, hence, increase the speed range, usually results in deterioration of certain other machine performance criteria [1], [2].

The concept of "electronic" pole changing between two pole numbers with an integer pole number ratio was initially suggested by Eichhofer *et al.* [3]. Further analysis of the technique of independently controlling the different coil group currents in a three-phase winding has been recently disclosed [4]. Based on this concept, a previous paper [5] reports a control scheme to extend the speed range for constant power operation of a four-pole induction machine. The proposed drive operates as a four-pole machine from zero speed until the end of its constant power range (3600 r/min for 2 pu overload torque capability). The constant-power speed range is extended by employing "electronic" pole changing to obtain two-pole operation. Due to flux canceling and poor winding utilization in two-pole operation, the standard 60° phase-belt stator-winding distribution is not employed in this drive. Fig. 1(a) shows the proposed drive stator-winding distribution which is a full-pitch double-layer 120° phase belt. The two coil groups per phase are connected separately, resulting in a six-terminal stator (1–6). As illustrated by Fig. 1(b), a six-leg inverter is needed to supply this machine. A coil group set consists of three coil groups belonging to three different phases, thus, coil groups 1, 4, and 5 form coil group set 1, while coil group set 2 consists of coil groups 2, 3, and 6. The number of poles of the machine is changed by merely reversing the direction (polarity) of the currents of one coil group set with respect to the currents of the other, as defined in Table I.

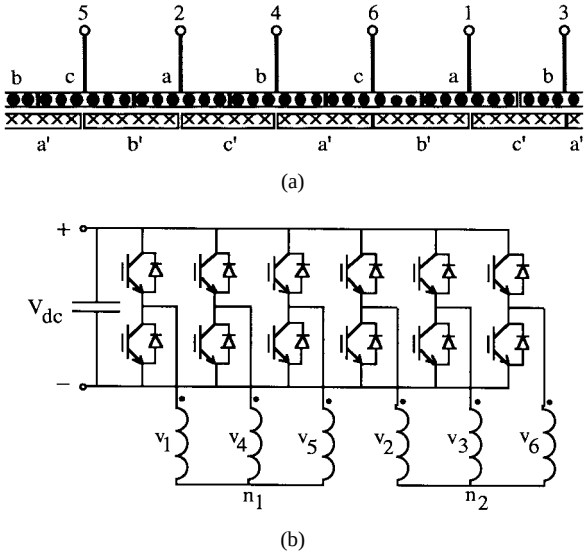

Fig. 1. Proposed induction machine drive. (a) Stator-winding distribution. (b) Inverter topology.

In this paper, the proposed drive capability is compared to conventional drives. A reference frame model for the six-coil-group machine is also derived. This model is utilized

Paper IPCSD 97–43, presented at the 1996 Industry Applications Society Annual Meeting, San Diego, CA, October 6–10, and approved for publication in the IEEE TRANSACTIONS ON INDUSTRY APPLICATIONS by the Industrial Drives Committee of the IEEE Industry Applications Society. Manuscript released for publication May 19, 1997.

M. Osama is with the Power Controls Program, Corporate Research and Development Center, General Electric Company, Schenectady, NY 12309 USA.

T. A. Lipo is with the Department of Electrical and Computer Engineering, University of Wisconsin, Madison, WI 53706-1691 USA.

Publisher Item Identifier S 0093-9994(97)07039-4.

TABLE I
COIL GROUPS CURRENT REFERENCES ACCORDING TO MODE OF OPERATION

	Ref. Current	4 pole mode	2 pole mode
Coil Group Set 1	i_1^*	i_a^*	i_a^*
	i_4^*	i_b^*	i_c^*
	i_5^*	i_c^*	i_b^*
Coil Group Set 2	i_2^*	i_a^*	$-i_a^*$
	i_3^*	i_b^*	$-i_c^*$
	i_6^*	i_c^*	$-i_b^*$

in analysis and control of the proposed induction machine drive.

II. POWER CAPABILITY COMPARISON

For the same magnetic structure, a 36- or 48-slot four-pole stator with conventional (60° phase belt) winding distribution, has a winding factor 1.15 times that in case of 120° phase-belt winding distribution. As a consequence, a 15% increase in the magnetizing component of the stator current is needed in a 120° phase-belt machine to maintain the same airgap flux density as a 60° phase-belt machine. By decomposing the stator current (I_s) into two components that are in time quadrature, the steady-state output power of an induction machine can be expressed as [6]

$$P_{\text{out}} = 3\omega_{rm}\frac{P}{2}\frac{L_m^2}{L_r}I_{s\phi}I_{sT} \tag{1}$$

where

ω_{rm} rotor speed (mech. r/s);
P number of poles;
L_m magnetizing inductance;
L_r rotor self inductance (referred to stator);
$L_{s\phi}$ flux component of stator current (A rms);
I_{sT} torque component of stator current (A rms).

From (1), the steady-state output power ratio between the proposed drive and conventional machines can be calculated at any operating point. Fig. 2 shows this power ratio at the same rated conditions (four-pole 60–Hz supply, rated flux density and current) as a function of the machine rating using data obtained from [7]. As demonstrated by the figure, the rated output power ratio approaches the winding factor ratio $(k_{w120}/k_{w60} = 0.866)$ as the machine rating increases due to the decrease in the per unit magnetizing current. In the following analysis, the proposed drive capability curves are evaluated for ratings of at least 100 hp, where the rated output power ratio is approximately 85%.

Fig. 3 shows the output power capabilities of the proposed induction machine drive, conventional four-pole and two-pole machines, all having the same outer dimensions and a 2-pu overload torque capability. The capability curves constraints are rated current throughout the operating range and the upper bound of the airgap flux density, yoke flux density and voltage being their rated values. The constant power range for the conventional four-pole machine ends at its slip limit (3600 r/min). Above that speed, constant power operation cannot be maintained; the current and, hence, the power has to decrease,

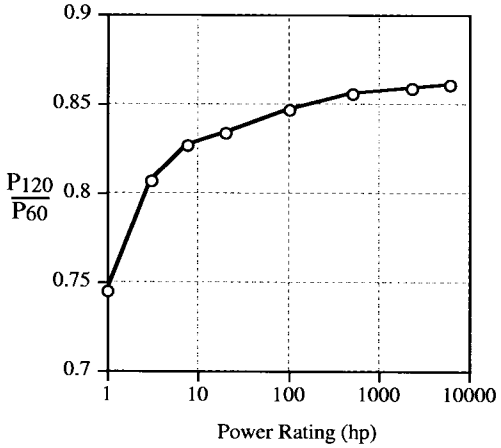

Fig. 2. Rated output power ratio for different machine ratings.

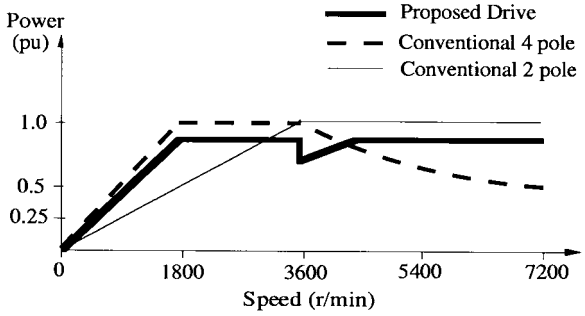

Fig. 3. Power capability comparison between proposed induction machine drive and conventional four-pole and two-pole machines having the same outer dimensions.

and the torque varies as the inverse of speed squared, as depicted in Fig. 3.

The steady-state peak per-phase airgap voltage can be defined as

$$V_m = \omega_e k_w N_{\text{ser}}\frac{A_{\text{tot}}}{P}B_g \tag{2}$$

where

ω_e supply angular frequency (elec. r/s);
k_w winding factor;
N_{ser} total number of series turns per phase;
A_{tot} total airgap surface area;
B_g average airgap flux density.

The ratio between the winding factors for two-pole and four-pole connections of 120° phase-belt winding is $k_{w2} \approx 0.8k_{w4}$. Thus, for the same magnetic structure and airgap flux density, the yoke flux density and airgap voltage for two-pole operation are 2 times and 0.8 times that of four-pole operation, respectively. Accordingly, when the mode of operation of the proposed drive changes (at 3600 r/min) from four-pole to two-pole, the applied voltage (hence, the power) has to drop by 20% for the core flux density not to exceed its rated value. In this case, as the speed is increased, the drive is operated in a constant torque mode until the rated voltage and power values are restored and, then, constant power operation is resumed. Though the proposed drive is derated (with respect to conventional machines) by about 15%, it has 70% more

torque capability than conventional two-pole machine drives at the lower speed range (below 1800 r/min) and maintains constant power and higher torque than the conventional four-pole machine drive at the higher speed range (4500–7200 r/min).

The need for twelve semiconductor devices instead of six (each rated at half the power rating of a three-leg inverter switch used for a conventional drive with the same rating) can be considered a disadvantage, but it could be noted that costing strategies of device manufacturers result in nearly the same cost for a given voltage and total voltampere rating regardless of the number of devices used. Hence, only a modest cost penalty is incurred (due to additional gate drive and control circuitry) by the use of a higher number of devices. Moreover, there are certain applications at higher power levels which already require twelve power semiconductor devices (each two devices connected in either series or parallel to form one switch).

III. Induction Machine Model

A. Coupled Circuit Model

The six-stator coil group three-phase machine can be modeled in the actual physical (rather than the transformed d–q) variables using the multiple coupled-circuit approach [8]. With each coupled circuit representing a coil group, the induction machine model equations in vector-matrix form are

$$[V_s] = [R_s][I_s] + \frac{d}{dt}[\lambda_s] \tag{3}$$

$$[\lambda_s] = [L_{ss}][I_s] + [L_{sr}][I_r] \tag{4}$$

$$[V_r] = [R_r][I_r] + \frac{d}{dt}[\lambda_r] \tag{5}$$

$$[\lambda_r] = [L_{sr}]^T[I_s] + [L_{rr}][I_r] \tag{6}$$

$$T_e = [I_s]^T \frac{\partial}{\partial \theta_{rm}}([L_{sr}])[I_r] \tag{7}$$

where

$$[V_s] = [v_1\ v_2\ v_3\ v_4\ v_5\ v_6]^T$$
$$[V_r] = [0\ 0\ 0\ 0\ 0\ 0]^T$$
$$[I_s] = [i_1\ i_2\ i_3\ i_4\ i_5\ i_6]^T$$
$$[I_r] = [i_7\ i_8\ i_9\ i_{10}\ i_{11}\ i_{12}]^T.$$

$[R_s]$ and $[R_r]$ are diagonal matrices with their elements being stator and rotor coupled circuits resistances, respectively.

Defining the winding function $N(\phi_m)$ as the MMF spatial distribution for 1 A of current [9], the mutual inductance between any two windings can be expressed in terms of their winding functions as

$$L_{ij} = \frac{\mu_0 r l}{g} \int_0^{2\pi} N_i(\phi_m) N_j(\phi_m)\, d\phi_m \tag{8}$$

where

- r outer radius of rotor or inner radius of stator;
- l axial length of the machine;
- g airgap length;
- ϕ_m angular position along the stator inner surface (mech. rad).

In order to obtain a closed-form coupled-circuit inductance expression, each stator coil group winding function is expanded as a Fourier series. Taking into account the dominant harmonics only, an approximate closed-form expression of all six coil groups winding functions can be written as

$$\begin{aligned}
N_1(\phi_m) &= N_{s1}\ \cos(\phi_m) + N_{s2}\ \cos(2\phi_m) + N_{s3}\ \cos(3\phi_m) \\
N_2(\phi_m) &= N_{s1}\ \cos(\phi_m - \pi) + N_{s2}\ \cos(2\phi_m) \\
&\quad + N_{s3}\ \cos(3\phi_m - \pi) \\
N_3(\phi_m) &= N_{s1}\ \cos\left(\phi_m - \frac{\pi}{3}\right) + N_{s2}\ \cos\left(2\phi_m - \frac{2\pi}{3}\right) \\
&\quad + N_{s3}\ \cos(3\phi_m - \pi) \\
N_4(\phi_m) &= N_{s1}\ \cos\left(\phi_m + \frac{2\pi}{3}\right) + N_{s2}\ \cos\left(2\phi_m - \frac{2\pi}{3}\right) \\
&\quad + N_{s3}\ \cos(3\phi_m) \\
N_5(\phi_m) &= N_{s1}\ \cos\left(\phi_m - \frac{2\pi}{3}\right) + N_{s2}\ \cos\left(2\phi_m + \frac{2\pi}{3}\right) \\
&\quad + N_{s3}\ \cos(3\phi_m) \\
N_6(\phi_m) &= N_{s1}\ \cos\left(\phi_m + \frac{\pi}{3}\right) + N_{s2}\ \cos\left(2\phi_m + \frac{2\pi}{3}\right) \\
&\quad + N_{s3}\ \cos(3\phi_m - \pi).
\end{aligned} \tag{9}$$

Though a coupled-circuit model is satisfactory for simulation purposes, the existence of cross-coupling terms and trigonometric nonlinearities makes it too laborious for analysis of the induction machine drive behavior and subsequent control of its performance. Thus, a reference frame model for the six-stator coupled-circuit three-phase machine is needed and is derived in this paper based on the concept of vector-space decomposition.

B. Vector-Space Decomposition

The conventional three-phase induction machine has three independent currents (in general), thus, it is modeled in a three-dimensional vector space defined by the transformation vectors $(d, q, 0)$. Similarly, the six-coil group machine is modeled in a six-dimensional vector space defined by six orthogonal transformation vectors. This vector space can be decomposed into four subspaces, as will be shown in this section. By utilizing the stator-winding representation of (9) and assuming a sinusoidal excitation with the phase angles equal to the spatial angles of the windings corresponding to them, the following basis vector is obtained:

$$\begin{aligned}
S_h(\omega t) = [&\cos(h\omega t)\ \cos(h\omega t - 3h\gamma)\ \cos(h\omega t - h\gamma) \\
&\cdot \cos(h\omega t - 4h\gamma)\ \cos(h\omega t - 2h\gamma) \\
&\cdot \cos(h\omega t - 5h\gamma)]^T
\end{aligned} \tag{10}$$

where $\gamma = \pi/3$.

The six transformation vectors are generated from the vector-space basis as follows.

- Setting $h = 1$ attains the first subspace $S_1(\omega t)$, which is the surface spanned by the spatial fundamental component (two-pole). Two orthogonal vectors (q_2 and d_2) are chosen in this subspace by setting $\omega t = 0\ \&\ -\pi/3$,

respectively in (10):

$$q_2 = \begin{bmatrix} 1 & -1 & \frac{1}{2} & -\frac{1}{2} & -\frac{1}{2} & \frac{1}{2} \end{bmatrix}^T$$
$$d_2 = \begin{bmatrix} 0 & 0 & -\frac{\sqrt{3}}{2} & \frac{\sqrt{3}}{2} & -\frac{\sqrt{3}}{2} & \frac{\sqrt{3}}{2} \end{bmatrix}^T. \quad (11)$$

- The second subspace $S_2(\omega t)$ is the surface spanned by the spatial second harmonic component (four-pole) which is obtained by setting $h = 2$. Two orthogonal vectors (q_4 and d_4) are selected from this subspace by setting $2\omega t = 0$ and $-\pi/2$, respectively:

$$q_4 = \begin{bmatrix} 1 & 1 & -\frac{1}{2} & -\frac{1}{2} & -\frac{1}{2} & -\frac{1}{2} \end{bmatrix}^T$$
$$d_4 = \begin{bmatrix} 0 & 0 & -\frac{\sqrt{3}}{2} & -\frac{\sqrt{3}}{2} & \frac{\sqrt{3}}{2} & \frac{\sqrt{3}}{2} \end{bmatrix}^T. \quad (12)$$

- The two remaining basis vectors are the zero vectors orthogonal to the dq two-pole and four-pole planes. Since the third harmonic and its multiples are zero-sequence components, the two one-dimensional (1-D) subspaces $S_3(\omega t)$ and $S_6(\omega t)$ are obtained by setting $h = 3$ and 6, respectively. One vector is selected from the collinear vectors spanning each subspace by choosing $h\omega t = \pi/4$ (to have equal vector norms for all basis vectors). The two zero vectors are

$$0_2 = \begin{bmatrix} \frac{1}{\sqrt{2}} & -\frac{1}{\sqrt{2}} & -\frac{1}{\sqrt{2}} & \frac{1}{\sqrt{2}} & \frac{1}{\sqrt{2}} & -\frac{1}{\sqrt{2}} \end{bmatrix}^T$$
$$0_4 = \begin{bmatrix} \frac{1}{\sqrt{2}} & \frac{1}{\sqrt{2}} & \frac{1}{\sqrt{2}} & \frac{1}{\sqrt{2}} & \frac{1}{\sqrt{2}} & \frac{1}{\sqrt{2}} \end{bmatrix}^T. \quad (13)$$

By varying ωt from 0 to 2π in all four subspaces and calculating the inner products between them, it can be proven that all four surfaces are mutually orthogonal and, thus, the six basis vectors spanning them are also all mutually orthogonal. These six vectors ($q_4 - d_4 - q_2 - 0_4 - 0_2$) define a stationary reference frame transformation matrix:

$$T(0) = \frac{1}{\sqrt{3}} \begin{bmatrix} 1 & 1 & -\frac{1}{2} & -\frac{1}{2} & -\frac{1}{2} & -\frac{1}{2} \\ 0 & 0 & -\frac{\sqrt{3}}{2} & -\frac{\sqrt{3}}{2} & \frac{\sqrt{3}}{2} & \frac{\sqrt{3}}{2} \\ 1 & -1 & \frac{1}{2} & -\frac{1}{2} & -\frac{1}{2} & \frac{1}{2} \\ 0 & 0 & -\frac{\sqrt{3}}{2} & \frac{\sqrt{3}}{2} & -\frac{\sqrt{3}}{2} & \frac{\sqrt{3}}{2} \\ \frac{1}{\sqrt{2}} & \frac{1}{\sqrt{2}} & \frac{1}{\sqrt{2}} & \frac{1}{\sqrt{2}} & \frac{1}{\sqrt{2}} & \frac{1}{\sqrt{2}} \\ \frac{1}{\sqrt{2}} & -\frac{1}{\sqrt{2}} & -\frac{1}{\sqrt{2}} & \frac{1}{\sqrt{2}} & \frac{1}{\sqrt{2}} & -\frac{1}{\sqrt{2}} \end{bmatrix}. \quad (14)$$

A more generalized transformation would express the machine variables in an arbitrary rotating reference frame. Such a reference frame would be rotating at a mechanical angular velocity of ω_m. The mechanical angular displacement of the reference frame ($\theta_m = \int \omega_m \, dt$) is chosen with respect to coil group 1 magnetic axis. For the two-pole surface, the mechanical and electrical angles are equal, thus, the two vectors q_2 and d_2 would rotate at an electrical angle $\theta_2 = \theta_m$. On the other hand, for the four-pole plane, the electrical angle is twice the mechanical angle, so q_4 and d_4 vectors rotate at an electrical angle $\theta_4 = 2\theta_m$. Hence, the four-pole dq plane (subspace) rotates at twice the electrical velocity of the two-pole plane; $\omega_4 = 2\omega_2$. The two zero vectors are independent of the reference frame angular displacement. The stator coil group variables are transformed to a vector space in the arbitrary rotating reference frame as shown in (15), shown at the bottom of the page, where f can represent either voltage, current, flux linkage, or electric charge, "c" is the abbreviation of cosine, "s" is the abbreviation of sine, and θ_2 and θ_4 are the electrical angular displacement of the two-pole and four-pole subspaces (planes), respectively, with respect to coil group 1 magnetic axis.

A similar transformation of the rotor variables to a vector space in the arbitrary rotating reference frame can be accomplished by

$$[f^{\theta}_{dqr}] = [T_r(\theta, \theta_r)][f_r]. \quad (16)$$

$$[f^{\theta}_{dqs}] = [T(\theta)][f_s]$$

$$\begin{bmatrix} f^{\theta}_{q4} \\ f^{\theta}_{d4} \\ f^{\theta}_{q2} \\ f^{\theta}_{d2} \\ f^{\theta}_{04} \\ f^{\theta}_{02} \end{bmatrix} = \frac{1}{\sqrt{3}} \begin{bmatrix} c(\theta_4) & c(\theta_4) & c\left(\theta_4 - \frac{2\pi}{3}\right) & c\left(\theta_4 - \frac{2\pi}{3}\right) & c\left(\theta_4 + \frac{2\pi}{3}\right) & c\left(\theta_4 + \frac{2\pi}{3}\right) \\ s(\theta_4) & s(\theta_4) & s\left(\theta_4 - \frac{2\pi}{3}\right) & s\left(\theta_4 - \frac{2\pi}{3}\right) & s\left(\theta_4 + \frac{2\pi}{3}\right) & s\left(\theta_4 + \frac{2\pi}{3}\right) \\ c(\theta_2) & -c(\theta_2) & -c\left(\theta_2 + \frac{2\pi}{3}\right) & c\left(\theta_2 + \frac{2\pi}{3}\right) & c\left(\theta_2 - \frac{2\pi}{3}\right) & -c\left(\theta_2 - \frac{2\pi}{3}\right) \\ s(\theta_2) & -s(\theta_2) & -s\left(\theta_2 + \frac{2\pi}{3}\right) & s\left(\theta_2 + \frac{2\pi}{3}\right) & s\left(\theta_2 - \frac{2\pi}{3}\right) & -s\left(\theta_2 - \frac{2\pi}{3}\right) \\ \frac{1}{\sqrt{2}} & \frac{1}{\sqrt{2}} & \frac{1}{\sqrt{2}} & \frac{1}{\sqrt{2}} & \frac{1}{\sqrt{2}} & \frac{1}{\sqrt{2}} \\ \frac{1}{\sqrt{2}} & -\frac{1}{\sqrt{2}} & -\frac{1}{\sqrt{2}} & \frac{1}{\sqrt{2}} & \frac{1}{\sqrt{2}} & -\frac{1}{\sqrt{2}} \end{bmatrix} \begin{bmatrix} f_1 \\ f_2 \\ f_3 \\ f_4 \\ f_5 \\ f_6 \end{bmatrix} \quad (15)$$

Each element in $T_r(\theta,\theta_r)$ is the same as in $T(\theta)$ with a change in the arguments, (θ_4) replaced by $(\theta_4-2\theta_{rm})$ and θ_2 replaced by $(\theta-\theta_{rm})$.

C. Reference Frame Model

1) Voltage Equations: Applying the transformation $T(\theta)$ to both sides of the stator coupled-circuit voltages (3) results in

$$[V_{dqs}]=[R_s][I_{dqs}]+[T(\theta)]\frac{d}{dt}([T(\theta)]^{-1})[\lambda_{dqs}]+\frac{d}{dt}[\lambda_{dqs}]. \tag{17}$$

Equation (17) can be expanded to obtain the stator voltage equations in arbitrary reference frame variables:

$$\begin{aligned}
v_{q4s}&=r_s i_{q4s}+\frac{d\lambda_{q4s}}{dt}+\omega_4\lambda_{d4s}\\
v_{d4s}&=r_s i_{d4s}+\frac{d\lambda_{d4s}}{dt}-\omega_4\lambda_{q4s}\\
v_{q2s}&=r_s i_{q2s}+\frac{d\lambda_{q2s}}{dt}+\omega_2\lambda_{d2s}\\
v_{d2s}&=r_s i_{d2s}+\frac{d\lambda_{d2s}}{dt}-\omega_2\lambda_{q2s}\\
v_{04s}&=r_s i_{04s}+\frac{d\lambda_{04s}}{dt}\\
v_{02s}&=r_s i_{02s}+\frac{d\lambda_{02s}}{dt}.
\end{aligned} \tag{18}$$

The transformed stator flux linkages are defined as

$$[\lambda_{dqs}]=[L_{dqss}][I_{dqs}]+[L_{dqsr}][I_{dqr}] \tag{19}$$

where

$$\begin{aligned}
[L_{dqss}]&=[T(\theta)][L_{ss}][T(\theta)]^{-1}\\
[L_{dqsr}]&=[T(\theta)][L_{sr}][T_r(\theta,\theta_r)]^{-1}.
\end{aligned}$$

By carrying out the transformations for the coupled-circuits inductances, (19) reduces to

$$\begin{aligned}
\lambda_{q4s}&=(L_{m4}+L_{ls})i_{q4s}+L_{m4}i_{q4r}\\
\lambda_{d4s}&=(L_{m4}+L_{ls})i_{d4s}+L_{m4}i_{d4r}\\
\lambda_{q2s}&=(L_{m2}+L_{ls})i_{q2s}+L_{m2}i_{q2r}\\
\lambda_{d2s}&=(L_{m2}+L_{ls})i_{d2s}+L_{m2}i_{d2r}\\
\lambda_{04s}&=L_{ls}i_{04s}\\
\lambda_{02s}&=(L_{m0}+L_{ls})i_{02s}+L_{m0}\cos(3\theta_{rm})i_{02r}
\end{aligned} \tag{20}$$

where

$$\begin{aligned}
L_{m4}&=3kN_{s2}^2\\
L_{m2}&=3kN_{sl}^2\\
L_{m0}&=6kN_{s3}^2\\
k&=\frac{\mu_0 rl\pi}{g}.
\end{aligned}$$

Equation (20) shows that there is no mutual inductance between the four-pole and two-pole equivalent windings.

By applying the transformation $T_r(\theta,\theta_r)$ to (5) and (6), expressions analogous to (18) and (20) are obtained for the rotor voltage and flux linkage equations in the arbitrary rotating reference frame.

2) Electromagnetic Torque: In the case of no neutral connections, the machine electromagnetic torque expression is deduced to be

$$\begin{aligned}
T_e&=[I_{dqs}]^T T(\theta)\frac{\partial}{\partial\theta_{rm}}([L_{sr}])[T_r(\theta,\theta_r)]^{-1}[I_{dqr}]\\
&=2(\lambda_{d4s}i_{q4s}-\lambda_{q4s}i_{d4s})+(\lambda_{d2s}i_{q2s}-\lambda_{q2s}i_{d2s}).
\end{aligned} \tag{21}$$

Equation (21) shows that the resultant machine torque is the superposition of two components, one due to the interaction of four-pole currents and fluxes and the second due the interaction of two-pole currents and fluxes. The interaction between four-pole and two-pole currents and fluxes does not produce any torque. This is partly due to the choice of the harmonic equivalent windings on the rotor as being stationary with respect to each other. This assumption is possible for the proposed drive, since the two-pole supply frequency is half the four-pole supply frequency, resulting in the four-pole and two-pole fields traveling at the same speed in space. Equation (21) is not valid for conventional line-supply contactor-based pole changing, where there is a pulsating torque component resulting from the interaction of the four-pole field with the two-pole field.

3) Radial Electromagnetic Force: While a combination of two- and four-pole fields does not interact to produce torque, radial forces are a concern. Chapman [11] has shown that two flux waves differing by two poles around the whole rotor periphery produce an unbalanced magnetic pull. Based on the reference frame model and applying the principle of virtual displacement, the radial electromagnetic force orthogonal components are

$$F_x=\frac{1}{2g}[I_{dq}]^T[Kx_{dq}][I_{dq}] \tag{22a}$$

$$F_y=\frac{1}{2g}[I_{dq}]^T[Ky_{dq}][I_{dq}] \tag{22b}$$

where

$$\begin{aligned}
Kx_{dqij}&=\frac{\mu_0 rl}{g}\int_0^{2\pi}N_{dqi}(\phi_m,\theta)N_{dqj}(\phi_m,\theta)\cdot\cos(\phi_m-\theta_2)\,d\phi_m\\
Ky_{dqij}&=\frac{\mu_0 rl}{g}\int_0^{2\pi}N_{dqi}(\phi_m,\theta)N_{dqj}(\phi_m,\theta)\cdot\sin(\phi_m-\theta_2)\,d\phi_m.
\end{aligned}$$

N_{dqi} is the winding function for reference frame variable i.

With the absence of neutral connections, the two orthogonal components of the radial electromagnetic force can be expressed in terms of airgap flux linkage as

$$F_x=\frac{M_{24}}{gL_{m4}L_{m2}}(\lambda_{q4m}\lambda_{q2m}+\lambda_{d4m}\lambda_{d2m}) \tag{23a}$$

$$F_y=\frac{M_{24}}{gL_{m4}L_{m2}}(\lambda_{q4m}\lambda_{d2m}-\lambda_{d4m}\lambda_{q2m}) \tag{23b}$$

where

$$M_{24}=\frac{3kN_{s1}N_{s2}}{2}=\frac{1}{2}\sqrt{L_{m4}L_{m2}}.$$

Note that the x and y directions (hence, F_x and F_y) are rotating with a rotational angle θ_2 in space (since they are attached to

the reference frame). The stationary horizontal and vertical components of the net radial force are

$$\begin{bmatrix} F_{x'} \\ F_{y'} \end{bmatrix} = \begin{bmatrix} \cos(\theta_2) & -\sin(\theta_2) \\ \sin(\theta_2) & \cos(\theta_2) \end{bmatrix} \begin{bmatrix} F_x \\ F_y \end{bmatrix}. \tag{24}$$

IV. Results

During the pole-changing transition, the buildup and decay of the four-pole and two-pole variables will not be instantaneous, but governed by their respective time constants. Consequently, a rotor flux transient exists, leading to a torque transient even if current regulation is maintained during the transition. The torque transient affects the electric drive speed, with the value of speed change determined by the motor and load inertia. As demonstrated by (23), the coexistence of four-pole and two-pole airgap fields during the pole-changing transition will also lead to a nonzero net radial force. This radial force transient will be detrimental to the motor bearings. Conventional bearings are not designed to withstand radial forces, and repeated transitions could significantly shorten their life span. In this section, the proposed drive performance during the pole-switching transition is investigated experimentally and using digital simulations.

For the experimental setup, a 4-kW induction machine is rewound to have the 120° phase-belt winding distribution shown in Fig. 1(a). The measured per-phase parameters for both four-pole and two-pole connections are listed in the Appendix. The machine is supplied from a six-leg CRPWM voltage-source inverter, the topology of which is shown in Fig. 1(b). Current regulation, as well as slip frequency control, is implemented using a MOTOROLA DSP56000 microprocessor. The digital simulations are based on the reference frame model derived in Section III, with the same parameters and operating conditions as the experimental setup.

Two different pole-changing transition schemes are compared in this paper. The first scheme is a step change in the reference frame current commands. The second transition scheme involves a ramp change in the current commands, where there is an overlap time during which i^*_{q4s} and i^*_{d4s} ramp down while i^*_{q2s} and i^*_{d2s} ramp up for four-to-two-pole transition and vice versa for two-to-four-pole transition. The slip frequency and current amplitude are kept constant throughout the operating range for both transition schemes. The electrical supply angles are chosen as

$$\theta_4 = \theta_s + 2\theta_{rm} \quad \text{and} \quad \theta_2 = \theta_s + \theta_{rm} \tag{25}$$

where θ_s is the slip angle (elec. rad), since

$$\theta_s \ll \theta_{rm}, \quad \theta_4 \approx 2\theta_2.$$

A. Step Transition

Fig. 4 shows the simulation results for the four-to-two-pole switching transition in the case of a step change in the reference frame current commands for a load torque of 1.4 N·m. The four-pole plane airgap flux linkage (λ_{4m}) decays exponentially at a rate governed by the four-pole mode rotor open-circuit time constant $(T_{r4} = 136 \text{ ms})$, while the two-pole plane airgap flux linkage (λ_{2m}) builds up according to the two-pole mode rotor open-circuit time constant $(T_{r2} = 221 \text{ ms})$. The interaction of these two field components results in a radial force vector rotating with an angle $(\theta_4 - \theta_2)$ and an amplitude $F = \sqrt{F_x + F_y}$. It is also clear from the figure that a step transition results in a large torque transient that even reaches a negative value. Figs. 5 and 6 present the experimental results in the case of a step transition. For the same slip frequency and current magnitude, four-pole operation has a higher back EMF,

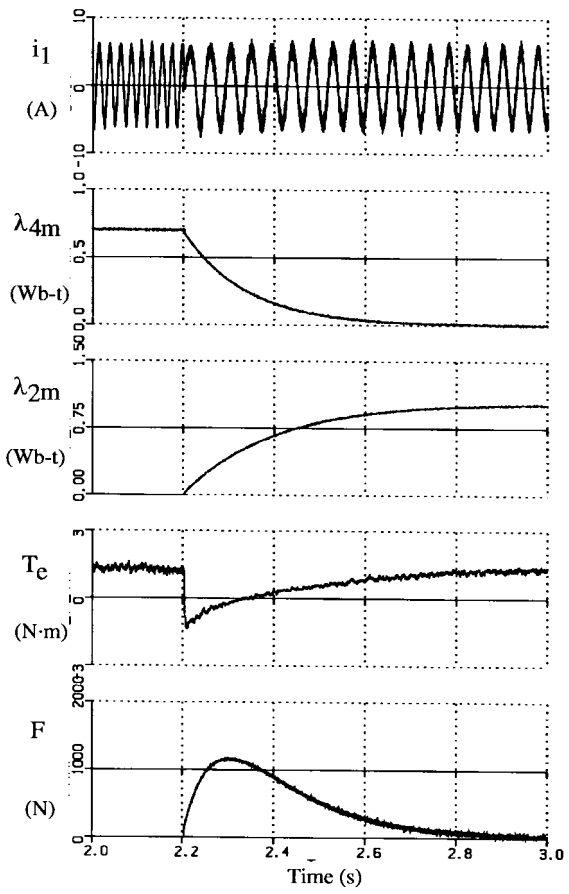

Fig. 4. Simulation results for pole-switching transition in the case of step change in stator-supply pole number.

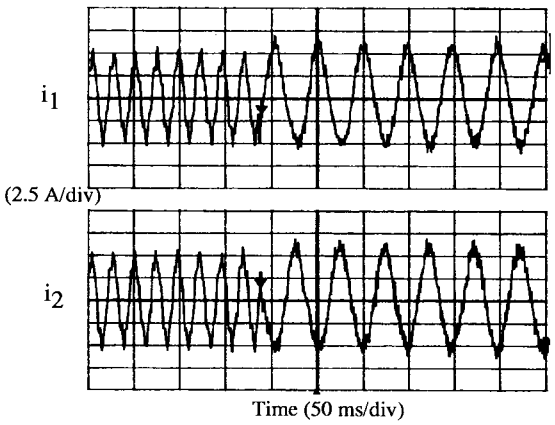

Fig. 5. Experimental results. Coil groups 1 and 2 currents during pole-switching transition in the case of step change in stator-supply pole number.

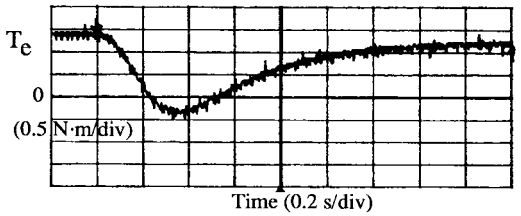

Fig. 6. Experimental results. Torque during pole-switching transition in the case of step change in stator-supply pole number.

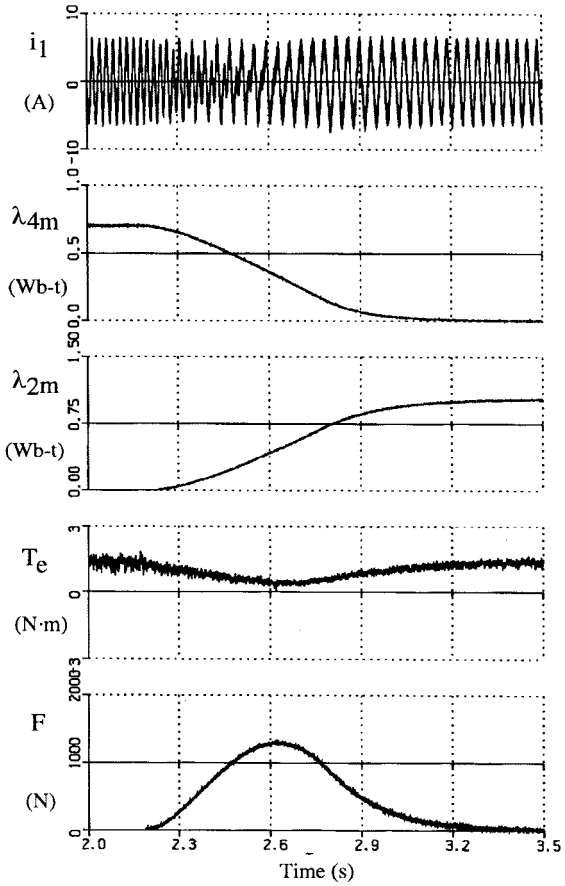

Fig. 7. Simulation results for pole-switching transition in the case of ramp change in stator-supply pole number.

resulting in current overmodulation, which does not exist in two-pole operation for this operating point. Comparing the torque transient of Fig. 6 to the simulation results (Fig. 4) shows close correlation with the exception of the initial decay rate.

B. Ramp Transition

Fig. 7 shows the simulation results for the pole-switching transition in the case of a ramp change in the reference frame current commands with an overlap time of 0.6 s. It is clear from the figure that this overlap time results in elongating the period during which λ_{4m} and λ_{2m} decay and rise, respectively, leading to a decrease in the torque transient. Meanwhile, the ramp transition profile has negligible effect on the radial force vector amplitude, but it extends the duration of the radial force transient. The experimental results for

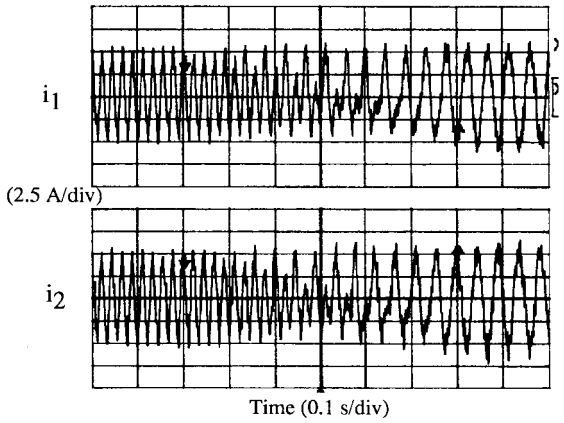

Fig. 8. Experimental results. Coil groups 1 and 2 currents during pole-switching transition in the case of ramp change in stator-supply pole number.

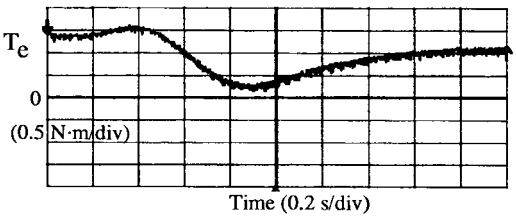

Fig. 9. Experimental results. Torque during pole-switching transition in the case of ramp change in stator-supply pole number.

ramp transition are presented in Figs. 8 and 9, where the torque trace shows an improvement over the case of a step transition (Fig. 6) and matches the simulation results of Fig. 7. The choice of 0.6 s overlap time is based on comparing the drive pole-switching performance for different overlap time values. A shorter overlap time led to a larger torque transient, while elongating the overlap time beyond 0.6 s had minimal improvement on the transient response.

V. Other Electronic Pole-Change Drives

The main disadvantage of the four/two-pole drive (existence of net radial forces) is eliminated in the case of any other drive with an integer pole number ratio, even during the pole-changing transition. By utilizing the same drive topology as the four/two-pole drive and changing the stator-winding distribution, any electronic pole-change drive with a pole number ratio of two can be achieved. The formulation of the induction machine model in this case can be attained by the same approach as in Section III. Based on the same principle, an eight/four-pole induction motor drive is currently being developed for an electric vehicle application by Meidensha Corporation [13].

By the appropriate stator-winding distribution, a pole-changing drive with three modes of operation (e.g., eight/four/two) can be theoretically attained. This drive would need 18 or 24 semiconductor switches without an increase in the total rating of the inverter. Due to the poor utilization of the magnetic circuit in at least one out of the three operation modes, the gain (if any) in the constant-power-speed-range capability is minimal in such a drive.

Based on the same winding distribution as that of a single-winding brushless doubly fed machine [14], [15], a six/two-pole drive can be realized. This drive would need two three-leg inverters, each operating during one mode only and, thus, the total inverter rating would be twice the machine rating.

VI. Conclusions

This paper presented an analysis and modeling of an induction motor drive that is based on electronic pole changing. The reference frame model derived specifically for this drive generates the same simulation results as previously obtained using a coupled-circuits model, with the advantage of having decoupled four-pole and two-pole $dq0$ variables, making it more suitable for analysis and control. Moreover, the viability of this model was proven by correlating its results to those obtained from the laboratory experiment. Two pole-changing transition schemes were compared. A ramp transition has the advantage of a lower torque transient than a step transition, but the duration of the resulting radial force transient is extended.

Appendix
Machine Parameters Used in the Experiment and Simulation Studies

Per phase parameter	4 pole connection	2 pole connection
Stator resistance	0.453 Ω	0.422 Ω
Rotor resistance	0.281 Ω	0.277 Ω
Stator leakage inductance	1.31 mH	1.15 mH
Rotor leakage inductance	1.31 mH	1.15 mH
Unsat. magnetizing induct.	40 mH	79 mH

References

[1] A. Boglietti, M. Lazzari, A. Tenconi, and C. Zimaglia, "Induction motor design criteria for traction application," in *Proc. European Power Electronics Chapter Symp.: Electric Drive Design and Applications*, 1994, pp. 543–548.

[2] A. Harson, P. H. Mellor, and D. Howe, "Design considerations for induction machines for electric vehicle drives," in *Proc. 7th Int. Conf. Electrical Machines and Drives*, 1995, pp. 16–20.

[3] H. Eichhofer, V. V. Sastry, and H. Weh, "Wechselrichtergespeiste Asynchronmachinen mit elektronischer Polumschaltung," ETZ, vol. 28, no. 5, pp. 116–118, 1976.

[4] M. Osama, "Modeling and applications of radial forces in induction machines," M.S. thesis, Dep. Elect. Eng., Univ. Wisconsin, Madison, 1994.

[5] M. Osama and T. A. Lipo, "A new inverter control scheme for induction motor drives requiring wide speed range," in *Proc. IEEE-IAS Annu. Meeting*, 1995, pp. 350–355.

[6] D. W. Novotny and T. A. Lipo, *Vector Control and Dynamics of AC Drives*. London, U.K.: Clarendon, 1996.

[7] R. Stern and D. W. Novotny, "A simplified approach to the determination of induction machine dynamic response," *IEEE Trans. Power App. Syst.*, vol. PAS-97, pp. 1430–1439, July/Aug. 1978.

[8] H. A. Toliyat and T. A. Lipo, "Analysis of a concentrated winding induction machine for adjustable speed drive applications, part 1: motor analysis," *IEEE Trans. Energy Conversion*, vol. 6, pp. 679–683, Dec. 1991.

[9] N. Schmitz and D. W. Novotny, *Introductory Electromechanics.* New York: Ronald, 1965.

[10] Y. Zhao and T. A. Lipo, "Space vector PWM control of dual three-phase induction machine using vector space decomposition," *IEEE Trans. Ind. Applicat.*, vol. 31, pp. 1100–1109, Sept./Oct. 1995.

[11] F. T. Chapman, "The production of noise and vibration by certain squirrel-cage induction motors," *Proc. Inst. Elect. Eng.*, vol. 61, no. 1, pp. 39–48, 1922.

[12] A. Chiba, T. Deido, T. Fukao, and M. A. Rahman, "Analysis of bearingless ac motors," *IEEE Trans. Energy Conversion*, vol. 9, pp. 61–67, Mar. 1994.

[13] M. Mori, Y. Kido, T. Mizuno, T. Ashikaga, I. Matsuda, and T. Kobayashi, "Development of an inverter-fed six- phase pole change induction motor for electric vehicles," in *Proc. 13th Int. Electric Vehicle Symp.*, Osaka, Japan, 1996, vol. 2, pp. 511–517.

[14] A. K. Wallace, R. Spee, and H. K. Lauw, "Dynamic modeling of brushless doubly-fed machines," in *Proc. IEEE-IAS Annu. Meeting*, 1989, pp. 329–334.

[15] R. Spee, A. K. Wallace, and H. K. Lauw, "Performance simulation of brushless doubly-fed adjustable speed drives," in *Proc. IEEE-IAS Annu. Meeting*, 1989, pp. 738–743.

Mohamed Osama (S'95–M'97) received the B.S. degree in electrical power engineering from Cairo University, Cairo, Egypt, in 1991 and the M.S. and Ph.D. degrees in electrical engineering from the University of Wisconsin, Madison, in 1994 and 1997, respectively.

In April 1997, he joined the Power Controls Program at the Corporate Research and Development Center, General Electric Company, Schenectady, NY. His areas of interest include analysis and design of electrical machines and modeling of ac motor drives.

Thomas A. Lipo (M'64–SM'71–F'87), for a photograph and biography, see this issue, p. 1153.